Monografías de la Real Academia de Ciencias de Zaragoza **34**, 73–86, (2010).

Curvature and burning velocity of Bunsen flame tips

G. García-Soriano, J. L. Castillo, P. L. García-Ybarra

Dept. Física Matemática y de Fluidos, UNED, Madrid, Spain

and

F. J. Higuera

E. T. S. Ingenieros Aeronáuticos, UPM, Madrid, Spain

Abstract

The burning velocity of a premixed flame propagating in a given flammable mixture is known to depend on the difference between the curvature of the flame and the so-called curvature of the flow, which is the strain rate of the flow of fresh gas along the normal to the flame divided by the burning velocity of the planar flame. The difference between the local burning velocity and the burning velocity of a planar flame in a gas at rest is proportional to the difference of the flame and flow curvatures. The proportionality factor is the product of the burning velocity of the planar flame and the Markstein length, which is an intrinsic property of the flame that characterizes its dynamics. The Markstein length can be determined experimentally by simultaneously measuring the curvature of the flame and the strain rate of the flow. To achieve this goal, we have set up a laminar jet burner and used two PIV systems to measure the gas flow velocity in two perpendicular planes normal to the flame. Each PIV system is composed by two Q-switched Nd:YAG pulse lasers (New Wave, maximum 120 mJ/pulse at 532 nm wavelength), a double-shuttered cross-correlation camera (PCO, 1392×1040 pixels) and a pulse generator (ILA GmbH) to synchronize all the components as well as the two PIV systems. Oil droplets are used for tracking the flow and the flame. They are formed by condensation after oil evaporation in a seeding chamber placed in the air line. Seeded air and fuel gas (CO, H_2, CH_4) are mixed in a settling chamber upstream of the burner and burned in a stationary Bunsen flame. The oil droplets evaporate in the flame preheating region, thereby allowing a dual tomography of the front.

1 Introduction

Accelerated widespread use of natural gas and other gaseous fossil fuels is causing serious concern about shortage and global climate change. This concern has prompted a renewed interest in alternative gas fuels such as gasification syngas, landfill gas, and others, which are gaseous mixtures containing different amounts of carbon monoxide, hydrogen, methane and other combustible gases diluted in carbon dioxide, nitrogen and some minor components [1, 2]. Increasing the efficiency in the use of these alternative fuels demands a thoughtful characterization of its combustion properties (see Ref. [3] and references therein).

The laminar burning velocity and the Markstein length are among the most important properties regarding the propagation and dynamics of a premixed flame (deflagration) front. The burning velocity of a planar premixed flame, $U_{_L}$, is a basic characteristic of a reactive mixture to be determined in terms of the composition and richness (equivalence ratio) of the mixture. On the other hand, stability conditions, turbulent propagation and other dynamic properties of a flame are controlled to a large extent by a single scalar magnitude, namely the Markstein length $\mathcal{L}$, whose value is also determined by the physico-chemical properties of the mixture. It has units of length and plays the role of a high wavenumber cutoff for the perturbations, stabilizing disturbances of small wavelength and thereby promoting smooth flame fronts. When $\mathcal{L}$ is not large enough, flame instability emerges leading to cellular flames. This instability originates in the thermal expansion of the gas when it goes through the preheating region of the flame; the so-called Darrieus-Landau mechanism. During its thermal expansion, each material element behaves as a volumetric source of fluid which distorts the flow and provides a feedback mechanism that modifies the flame shape (see Ref. [4] for a review).

Gas flow inhomogeneities modify the local convective-diffusive balance inside the flame and cause a stretching of the flame front. Analysis [5] shows that, in certain conditions, there is a linear relation between the rate of stretching of the flame (the logarithmic derivative of the area $\delta\sigma$ of an element of the flame front) and the change of its local burning velocity, U_n, relative to the burning velocity of the planar flame $U_{_L}$. The Markstein length is the proportionality constant appearing in this linear relationship [5]:

$$U_{_L} - U_n = \mathcal{L}\ \frac{1}{\delta\sigma}\frac{\mathrm{d}\delta\sigma}{\mathrm{d}t}. \tag{1}$$

Further, the rate of stretching of an element of the flame is the sum of two contributions,

$$\frac{1}{\delta\sigma}\frac{\mathrm{d}\delta\sigma}{\mathrm{d}t} = -2U_{_L}\mathcal{C} - \boldsymbol{n}\cdot\boldsymbol{\nabla v}\cdot\boldsymbol{n}. \tag{2}$$

The first term on the right-hand side of (2) is the effect of the front curvature for a flame moving with a normal velocity $U_{_L}$. Here $\mathcal{C} = \frac{1}{2}(1/R_1 + 1/R_2)$ is the mean curvature of the

front, with R_1 and R_2 denoting the curvature radii of two normal sections of the surface perpendicular to each other. The second term on the right-hand side of (2) is the rate of stretching of a material surface in the shape of the flame immersed in the velocity field $\boldsymbol{v}$ of the fresh gas upstream of the flame. Here $\boldsymbol{n}$ is a unit vector normal to the surface.

The above expressions have been rigorously obtained in the asymptotic limit of an infinitely thin flame with large activation energy [5]. This theory also provides an expression for the Markstein length in terms of the physico-chemical properties of the gas. However, the question arises of how to use these results for a real flame of finite thickness. This question has been satisfactorily answered in Ref. [6], where several numerical examples are used to show that the upstream flow velocity (i.e., the *outer* solution of the asymptotic description) has to be extrapolated to the luminous region of the flame to apply Eq. (2).

In principle, the value of the Markstein length can be obtained from (1) if the local burning velocity and the flame and flow geometry can be determined experimentally. The experimental task can be further simplified if the experiment is designed in such a way that only one of the two contributions to the flame stretching discussed above is present. In previous works, this goal was achieved by using spherically (inward or outward) propagating flames [7] and with a flame in a stagnation flow configuration. In the first case only the front curvature term remains, whereas in the second case the flame is flat and the only contribution comes from the straining flow [8].

In the present work, a jet burner leading to a Bunsen-like flame has been selected to carry out the experiments. This kind of system allows the simultaneous measurement of the planar flame propagation velocity (from the angle of the flame to the flow in the region where the flame is conical) and the local normal burning velocity and curvature radius at the flame tip.

2 Preliminary considerations

The flame and flow curvatures have only a small effect in substantial regions of the flames produced in our burner. Before proceeding to the experimental determination of the Markstein length, it is therefore appropriate to briefly examine the flow and the flame shape when the burning velocity is taken to coincide with $U_{_L}$. More complete accounts of the aerodynamics of a Bunsen flame can be found in Refs. [9-28].

The density of the gas decreases across the flame from its value ρ_u in the fresh gas to a certain value ρ_b in the burnt gas, but it is uniform at each side of the flame. The density ratio $\epsilon = \rho_b/\rho_u$ is a fairly small number, in the range of 0.1–0.2 for typical flames.

Buoyancy forces have only a small effect in the dynamics of the burnt gas because the Froude number $\rho_b u_b^2/\rho_u g a$, where a is the radius of the burner nozzle (see following section) and $u_b = U_{_L}/\epsilon$ is the characteristic velocity of the burnt gas, is large of the order

of 25 for typical methane or propane flames and $a = 1$ cm.

The characteristic velocity of the fresh gas ahead of the flame is of the order of the injection velocity U_0, which will be taken to be uniform at the outlet of the nozzle on the assumption that the boundary layer around the wall of the nozzle is thin compared to its radius. Pressure variations of order $\rho_u U_0^2$ would occur in the fresh gas if velocity variations of order U_0 exist, though our experiments and others suggest that the velocity of the fresh gas is nearly uniform in many cases.

The velocity U_0 must be larger than a certain minimum to avoid flash back of the flame, but the ratio $U_0/U_{_L}$ is otherwise a free parameter whose value determines the aspect ratio of the flame. The height of the flame above the nozzle is $h = O\left[(U_0/U_{_L})a\right]$, which is large compared to the radius of the nozzle if $U_0/U_{_L}$ is large.

Mass and momentum conservation conditions across a stationary flame read

$$\rho_u u_{1n} = \rho_b u_{2n}, \tag{3}$$

$$p_1 + \rho_u u_{1n}^2 = p_2 + \rho_b u_{2n}^2, \tag{4}$$

$$u_{1t} = u_{2t}, \tag{5}$$

where subscripts 1 and 2 denote conditions immediately upstream and downstream of the flame and subscripts n and t denote the components of the velocity normal and tangent to the flame. If $u_{1n} = U_{_L}$ constant, then $u_{2n} = U_{_L}/\epsilon$, which is fairly large compared to $U_{_L}$. Similarly, the term $\rho_b u_{2n}^2$ in the normal momentum condition (4) is larger than the term $\rho_u u_{1n}^2$ by a factor $1/\epsilon$, so that the pressure jump across the flame is $p_2 - p_1 \approx -\rho_u u_{1n}^2/\epsilon$, which is a negative constant if the normal velocity of the flame is $U_{_L}$.

Velocity variations of order $U_{_L}/\epsilon$, leading to pressure variations of order $\rho_b U_{_L}^2/\epsilon^2$, should be expected in the burnt gas as it turns to become nearly vertical. These pressure variations are transmitted across the flame and affect the flow of the fresh gas. Their effect, however, is small when U_0 is large compared to $U_{_L}/\epsilon^{1/2}$, because $\rho_u U_0^2 \gg \rho_b U_{_L}^2/\epsilon^2$. The flow of fresh gas is then nearly uniform and the flame is a slender cone of semi-angle $U_{_L}/U_0 \ll 1$.

The axial and radial components of the velocity of the gas emerging from a slender flame are U_0 and $U_{_L}/\epsilon$, respectively, from conditions (3) and (5) and the condition that the flame surface is nearly vertical. Continuity requires that the radial velocity of the burnt gas decrease as the inverse of the distance to the symmetry axis as the gas moves away from the flame. From Bernouilli's equation, this deceleration is accompanied by an increase of pressure, which is equal to $\frac{1}{2}\rho_b U_{_L}^2/\epsilon^2$ at distances from the flame large compared to its local radius. Since the angle of the flame to the vertical is small, this increase of pressure occurs nearly uniformly along the flame and causes little variation of the axial velocity of the gas. The streamlines bend upwards and the flow becomes quasiunidirectional in a region around the flame whose radius is $R_b = a/\epsilon^{1/2}$, from the

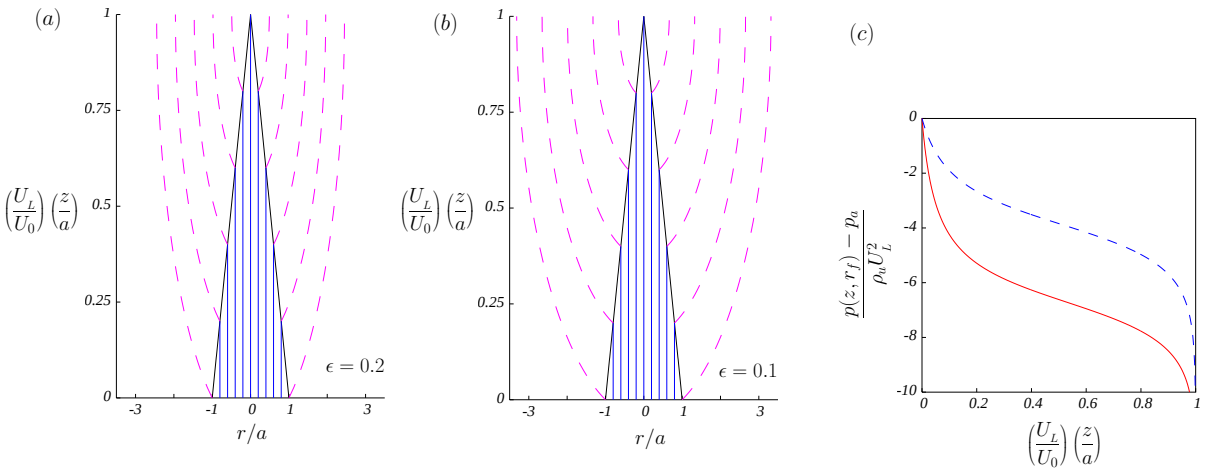

Figure 1.— (a) and (b): Conical slender flames and streamlines of the flow for two values of the burnt-to-fresh gas density ratio; $\epsilon = 0.2$ in (a) and 0.1 in (b). (c): Pressure of the burnt gas on the flame for $\epsilon = 0.1$ (solid) and 0.2 (dashed).

condition that the upward mass flux of burnt gas ($\pi R_b^2 \rho_b U_0$) should be equal to the mass flux issuing from the nozzle ($\pi a^2 \rho_u U_0$); see, e.g., Ref. [26].

Analysis of the flow of the burnt gas determines the velocity and pressure distributions as [28]

$$u_b = U_0, \qquad v_b = \frac{U_{_L}}{\epsilon}\frac{r_f}{r}, \qquad p - p_a = -\frac{1}{2}\rho_u U_{_L}^2 \left(\frac{1}{\epsilon}\frac{r_f^2}{r_s^2}\frac{r_s^2 - r^2}{r^2} + \ln\frac{r_s^2}{r^2}\right), \tag{6}$$

where u_b and v_b are the axial and radial components of the velocity of the burnt gas, p_a is the pressure of the ambient gas, r is the distance to the symmetry axis, and

$$r_f(z) = a\left(1 - \frac{U_{_L}}{U_0}\frac{z}{a}\right) \quad \text{and} \quad r_s(z) = a\left[1 + \frac{1}{\epsilon}\frac{U_{_L}}{U_0}\frac{z}{a}\left(2 - \frac{U_{_L}}{U_0}\frac{z}{a}\right)\right]^{1/2} \tag{7}$$

are the surfaces of the flame and the shear layer between the burnt gas and the quiescent ambient gas for $0 \le (U_{_L}/U_0)(z/a) \le 1$. Here z is the vertical distance above the nozzle.

Some streamlines of this flow are displayed in Fig. 1(a,b), and the pressure acting on the flame, $p(r = r_f(z))$, is shown in Fig. 1(c). As can be seen, this pressure decreases with distance along the flame, which causes an acceleration of the fresh gas in line with the experimental results discussed below.

The flame would cease to be slender when U_0 becomes of the order of $U_{_L}$. The following conditions should be satisfied for a stationary flame with a small value of ϵ to exist in this case. First, since the component of the velocity tangent to the flame is continuous while the component normal to the flame increases by a factor $1/\epsilon$ on crossing the flame, the burnt gas should emerge with a uniform velocity $U_{_L}/\epsilon$ normal to the flame. Second, since pressure variations of order $\rho_b U_{_L}^2/\epsilon^2$ are not admissible in the fresh gas, the surface of the flame should nearly coincide with the isobar $p = p_a$ from the point of view of

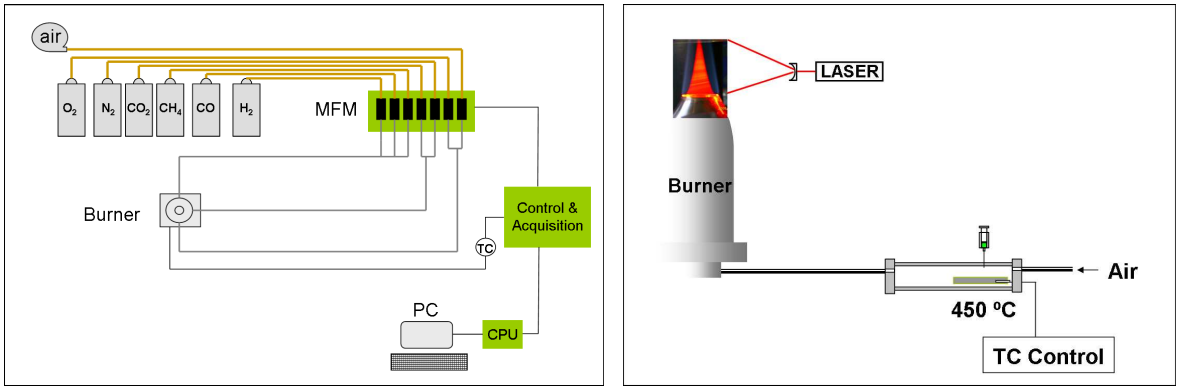

Figure 2.— Sketch of the laminar jet burner.

the burnt gas. The total pressure would then be nearly uniform in the burnt gas and the vorticity would be nearly zero. However, the flow cannot apparently proceed away from the flame under these conditions without causing inadmissible pressure and velocity variations, which casts doubts on the possible existence of a stationary flame.

3 Experimental setup

Our laminar jet burner consists of a plenum chamber where metered fluxes of gases (mass flow controllers from Bronkhost High-Tech) coming from different lines (left-hand side panel of Fig. 2) are mixed in the required proportions. The mixture is fed to a vertical tube fitted with various honeycomb structures and damping grids to uniformize the flow, and ended in a convergent nozzle of 2 cm exit diameter. The flame is ignited and attached to the rim of this nozzle.

The tracers required for PIV and flame tomography are olive oil droplets formed by evaporation-condensation of a 100:1 oil-water emulsion in a seeding camera placed in the air line (right-hand side panel of Fig. 2). These oil droplets evaporate on reaching the transport region of the flame, thus serving the intended dual purpose.

Figure 3 is a sketch of the setup of the crossed-plane PIV and tomographic imaging system for our jet burner. It consists of two 532 nm wavelength Nd:YAG lasers (New Wave 120XT), sheet-forming emission optics, two CCD cameras (PCO PixelFly 1392×1040 pixels) with Nikon automatic macro lenses, and pulse and delay generators for synchronizing all these devices. Each camera is focused perpendicularly to a laser sheet on a window of about 22×30 mm, giving a resolution in the order of 46 pixels/mm.

A single PIV is used in the simple case of an axisymmetric Bunsen flame. The light sheet is then vertical through the axis of the burner, and time shifts and pulse delays are fitted to the flow speed and size of the region of interest following standard practise for the cross-correlation method. Typical inter-pulse times are of the order of 70 μs. Cross-correlation computations are done with the ViDPIV software.

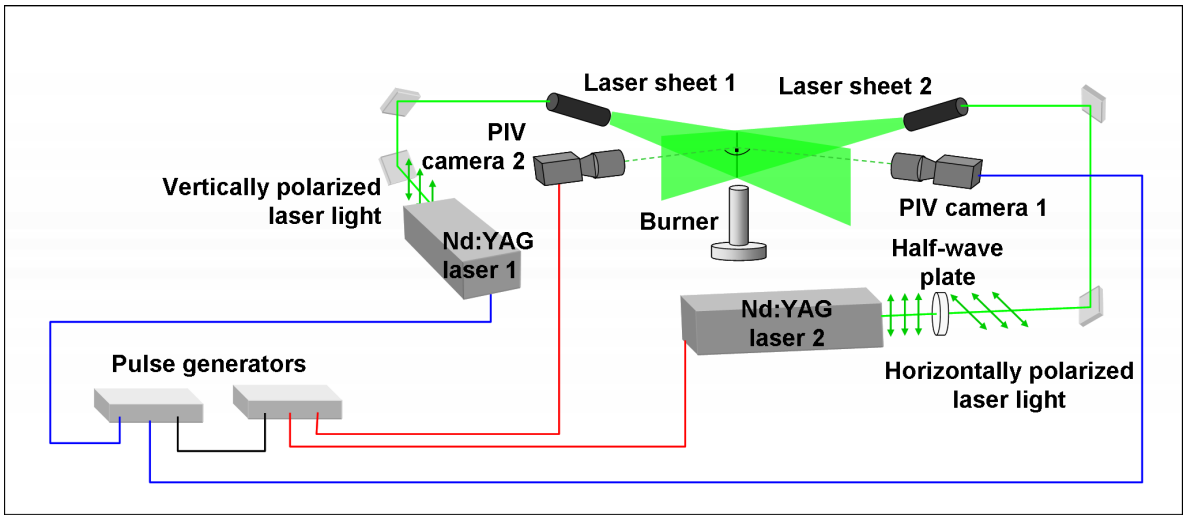

Figure 3.— Dual PIV system.

More complex flame configurations require that the two PIV systems be simultaneously used to try to measure the mean curvature of the flame front and all the required components of the velocity gradient tensor in Eq. (2). An added difficulty appears in this case because the light of each laser is scattered by the tracers and reaches both cameras for any realizable setting of the time delays. This spoils the correlation between pairs of images on which the method relies. The problem has been documented elsewhere (see Refs. [29, 30]), as well as two possible solutions. One of these is to polarize the two laser beams in perpendicular planes by means of a half-wave plate inserted in one of the laser paths (Fig. 3), and set polarization filters in front of the cameras that let pass only the light of the appropriate laser. The method works as far as the scattering on the tracers does not change the polarization of the incident light. The second possible solution relies on a careful choice of the timing of the two systems and the use of an electromechanical shutter in the camera of the system that is triggered first. Further details can be found in the references given above.

The left-hand side panel of Fig. 4 shows a photo of a rich butane-air flame stabilized in the burner. The excess fuel left behind the main premixed flame burns in this case with the oxygen of the air in an outer diffusion flame that appears as a faint bluish surface in the photo. A standard geometrical method (see, e.g. Ref. [21]) gives the burning velocity as the projection of the velocity of the fresh gas normal to the premixed flame, as sketched in the figure.

The central panel of Fig. 4 is a sample image (in negative) of the laser light scattered by the oil droplets in the fresh gas stream, as recorded by the PIV camera. The outer outline is due to the radiation emitted by the flame in the band of frequencies that pass through the filter set in front of the camera. Since the oil droplets evaporate at a fairly

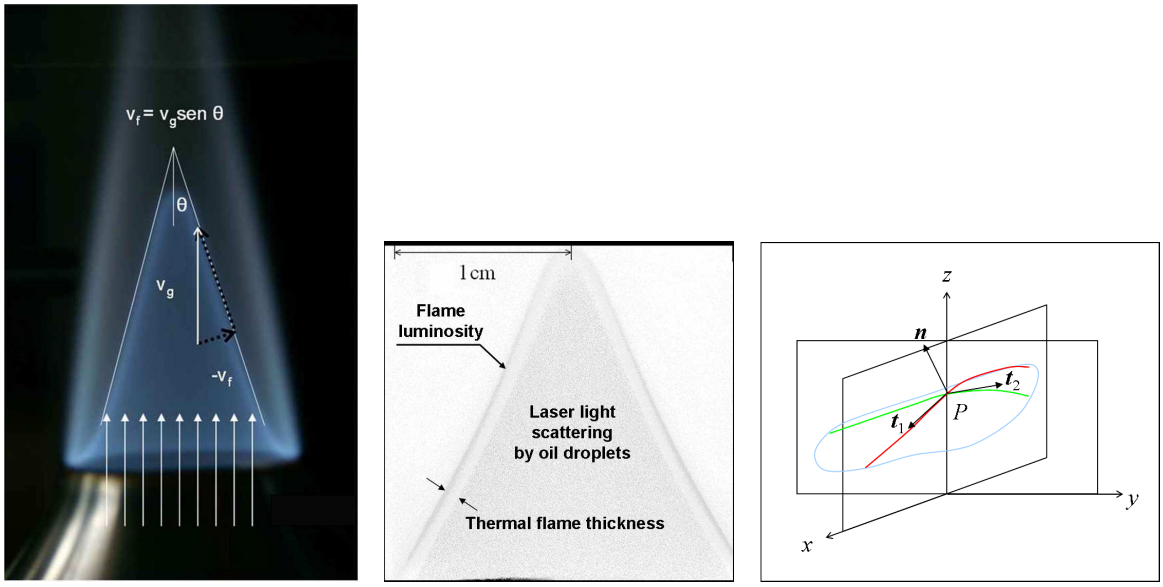

Figure 4.— Images of the flame and measurements of the burning velocity and the curvature.

low temperature, immediately upon entering the flame, while the radiation from the flame comes from nearly its reaction region, the two sources can be distinguished on the image, and the light strip between them gives an idea of the thermal thickness of the flame. A quantitative assessment of this thickness would require some caution, however, because the light emitted by the flame does not come only from the plane illuminated by the laser.

The right-hand side panel of Fig. 4 illustrates the geometrical construct used to measure the curvature radii of the sections of the flame determined by the two perpendicular laser sheets. Notice that, in general, these sections are not normal sections of the surface. The sum of the two measured curvatures gives the mean curvature of the flame front only when the normal to the flame $\boldsymbol{n}$ is contained in both laser sheets. Since the laser sheets are vertical in the configuration of Fig. 3, this condition is satisfied only when P is a local extreme on the flame surface.

4 Results and discussion

We present in this section some preliminary results obtained in the rig described above. A series of experiments were conducted with a rich mixture of methane and air at an equivalence ratio $\phi = 1.2$. Rich flame conditions were selected to take advantage of an stabilizing effect brought about by the outer diffusion flame where the excess methane is burnt. This flame induces an upward flow around the inner premixed flame, acting somehow as a coflow that sweeps the eddies of the surrounding shear layer before they can affect much the premixed flame. However, some flickering of the flame tip remains even under such favorable conditions, which greatly perturb the experiments. Its persistence

	U_0 (cm/s)	h (cm)	U_L (cm/s)
Case 1	$57.9 \pm 3\%$	2.2	30.5
Case 2	$51.7 \pm 6\%$	1.8	30.1
Case 3	$44.1 \pm 7\%$	1.3	32

Table 1.— Summary of experimental results.

suggests that the origin of the flame tip oscillation might not be in the instability of the shear layer; see further comments at the end of this section. A vertical tube concentric with the burner was arranged above the flame to generate a chimney effect that further stabilizes the flow.

In the experiments, a controllable fraction of the premixed gas stream can be diverted to a secondary burner to obtain conical flames with different cone angles for a given mixture. Results for three cases with different velocities at the nozzle outlet (U_0) are summarized in Table 1. In all cases this velocity is uniform except for a viscous boundary layer about 2 mm thick. The third column of Table 1 gives the height of the flame above the nozzle (h).

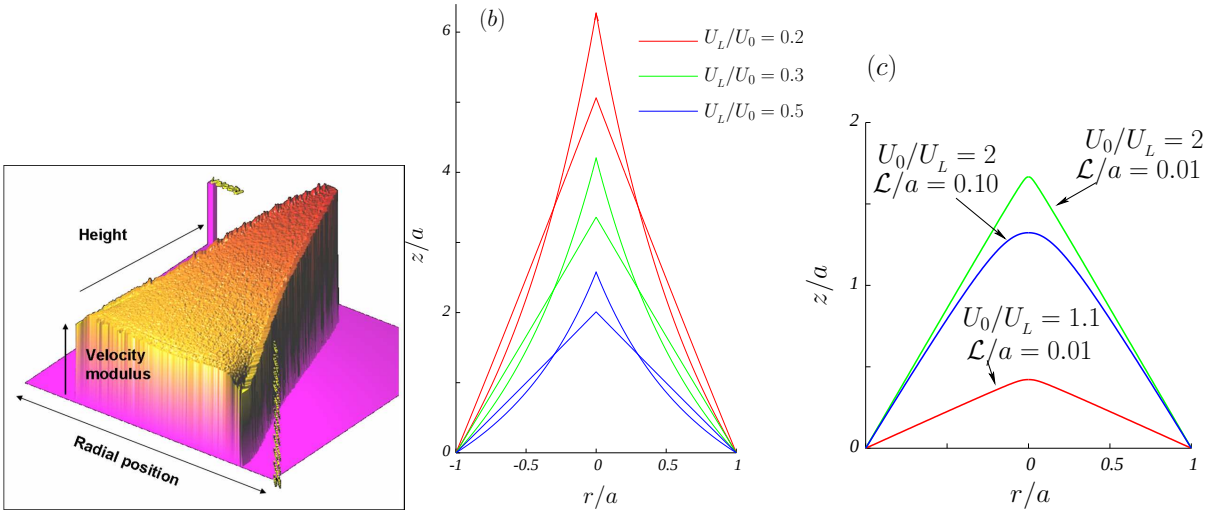

Figure 5.— (a) PIV map of velocities upstream of a Bunsen flame, showing the plug flow at the outlet of the burner and the increase of the gas velocity with height. (b) Shape of a Bunsen flame with constant burning velocity. The flame is conical in a uniform plug flow and bends upward in a flow with linearly increasing velocity. (c) Rounded tip of a Bunsen flame with a positive Markstein length in a uniform flow.

A sample map of the modulus of the velocity measured in the fresh gas with PIV is shown in Fig. 5(a). Remarkably, the vertical velocity always increases linearly with

height (z) independently of radial position. If velocities and distances are scaled with the values of U_0 and h in the second and third columns of Table 1, then all the velocity profiles collapse, within the experimental error, onto

$$\frac{u}{U_0} = 1 + B\,\frac{z}{h} \tag{8}$$

with

$$B = 0.5 \pm 10\%. \tag{9}$$

The vertical acceleration of the gas causes a contraction of the streamlines that changes the shape of the flame. Computed shapes of axisymmetric constant burning velocity flames in the linear velocity field (8) are shown in Fig. 5(b) for some values of $U_{_L}/U_0$. These shapes are to be compared with the experimentally observed flame of Fig. 4. Fig. 5(c), on the other hand, shows the effect of the Markstein length at rounding the tip of the flame in a uniform gas stream.

The curvature of the meridional section of the flame complicates the extraction of the burning velocity $U_{_L}$ from the experimental data. In principle, flame shapes computed for different values of $U_{_L}/U_0$ should be fitted to the visualized flames in a region away from its tip and its base where the burning velocity is expected to be constant. Fortunately, the simple projection rule mentioned above gives reasonable results, similar to those of the more complex fitting method, if it is applied to the upper part of the flame, where it is nearly a cone. Values of the burning velocity obtained in this manner are given in the fourth column of Table 1. The average value of the planar flame velocity is

$$U_{_L} = 31 \pm 10\% \quad \text{cm/s} \tag{10}$$

for a methane-air flame with $\phi = 1.2$, which compares well with the values found in the literature [6].

We turn now to the determination of the Markstein length by separately measuring the two terms on the right-hand side of (2) at the tip of the flame, on the axis of the burner. At this particular point, the last term of (2) is simply $-\partial u/\partial z = -BU_0/h$, from (8). As stated in Refs. [6, 8], the front curvature to use in (2) is that of the reaction layer of the flame, where the chemical reactions occur. (The curvature of the flow is also to be extrapolated to this layer from its distribution in the fresh gas, but this is of no consequence in our case because BU_0/h is a constant.) The reaction layer is infinitely thin in the asymptotic theory leading to (1) and (2), but evidently it has a finite thickness in reality, which makes the problem undetermined. The computational study performed by Davis et al. [6] shows that a experimental definition of the position of the reaction layer that gives good agreement with the asymptotic theory is to set it close to the position of the peak of the radical CH, which goes with the luminosity of the flame.

In our experiment, the exposition of the second picture taken by the PIV camera is long enough to neatly detect this luminous layer, and the curvature of the flame at the tip is measured by fitting a sphere to the outline of the luminous layer.

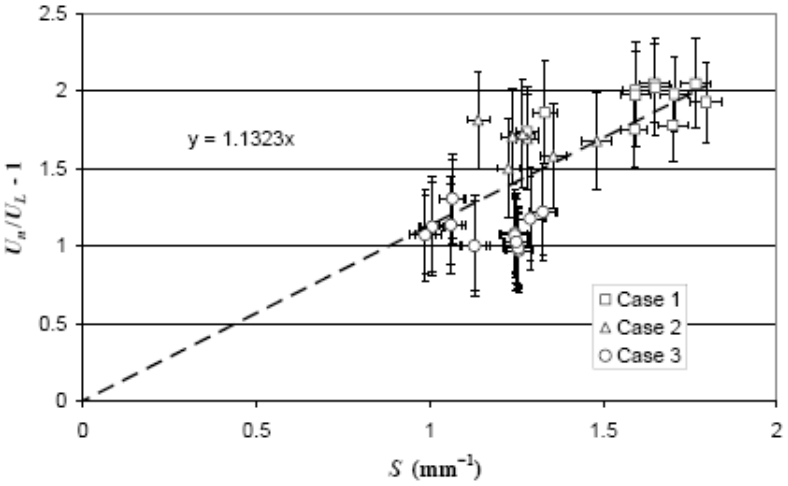

Figure 6.— Experimental correlation between burning velocity and rate of stretch at the tip of the flame.

In summary, the right-hand side of (2) at the tip of the flame is $-U_{_L} S$, where

$$S = \frac{2}{R} + \frac{B}{h} \tag{11}$$

and R is the radius of the fitting sphere. Equation (1) can then be rewritten as

$$\frac{U_n}{U_{_L}} - 1 = \mathcal{L}\, S. \tag{12}$$

Experimental data in the ($U_n/U_{_L}$, S) plane are shown in Fig. 6. Linear regression in this plane gives the approximate experimental value

$$\mathcal{L} = 1.1 \pm 20\% \quad \text{mm} \tag{13}$$

for the Markstein length.

The ratio of the Markstein length to the radius of the burner is $\mathcal{L}/a = 0.11$. This value and the value of the velocity ratio for Case 1 ($U_0/U_{_L} = 1.87$) are not far from the values used in one of the computations displayed in Fig. 5(c). The shape of the flame predicted by this computation compares reasonably well with the shape observed in the experiment.

Comparison with other results in the literature is best made in terms of the dimensionless Markstein number $\mathcal{M} = \mathcal{L}/l_t$, where $l_t = D_{th}/U_{_L}$ is the thermal thickness of the flame. Here $D_{th} = 0.225$ cm^2/s is the thermal diffusivity of the methane-air mixture and $U_{_L}$ is the planar flame velocity (10). For our mixture, $l_t = 7 \times 10^{-3}$ cm and

$$\mathcal{M} = 15 \pm 20\%. \tag{14}$$

Values of the Markstein number derived from measurements in the burnt gas, rather than in the fresh gas used here, are collected in Ref. [6] for a variety of conditions, though not for the particular mixture used in our experiment. These results and the computational results for the fresh gas in Ref. [6] show that the Markstein number as a function of the equivalence ratio reaches a maximum at about the value $\phi = 1.2$ used in our experiments. However (14) is about twice as large as the peak Markstein number in Ref. [6], a large discrepancy which we cannot presently explain and will demand exhaustive analysis and testing of our experimental methodology for a range of values of the equivalence ratio.

It may be noted that a Bunsen flame had never been used before to study the effect of flame stretching, despite it being one of the most familiar configurations in combustion. The tip of a Bunsen flame is peculiar in this respect because the contributions of surface curvature and flow strain both lead to an increase of the local burning velocity, and there might be an intrinsic oscillatory behavior associated to such condition. This may be seen as follows. Notice first that the linear increase of the velocity of the fresh gas with streamwise distance ahead of the flame would render a planar flame unstable because any displacement of the flame about its equilibrium position would lead to flash-back or blow-up. At the tip of a Bunsen flame, on the other hand, the curvature of the front increases (resp. decreases) when the flame shifts upward (resp. downward), causing the velocity of the flame to increase (resp. decrease) and thus oppose the initial shift. Therefore the variation of the front curvature tends to restore the flame to its equilibrium position, but it does so at the price of making the system oscillatory. This may be the reason behind the observed unsteadiness of the flame tip. We suggest, tentatively, that it may also be responsible for part of the observed discrepancy between (14) and other results in the literature, as the velocity of the oscillatory flame relative to the burner should be taken into account to properly evaluate U_n. Preliminary work in this direction shows, however, that this velocity is small compared to the velocity of the gas.

5 Conclusions

An experimental setup has been devised to simultaneously measure the burning velocity and the Markstein length of premixed flames in various flammable mixtures. A dual PIV system and flame tomography are used to determine the curvature of the flame and the strain rate of the fresh gas flow, on which the Markstein length depends. Preliminary results obtained for a rich methane-air mixture in the Bunsen flame configuration are presented and discussed. The measured burning velocity agrees well with known results, but the measured Markstein length shows a considerable discrepancy with results existing for similar mixtures. The possible causes of this discrepancy are discussed.

Acknowledgments.

This work was supported by the Comunidad de Madrid through project COMLI-MAMS, S-0505/ENE-229.

References

[1] ec.europa.eu/energy/library/599fi_en.pdf

[2] www.epa.gov/outreach

[3] C. Serrano, J. J. Hernandez, C. Mandilas, C. G. W. Sheppard and R. Woolley, Int. J. Hydrogen Energy 33, 851 (2008).

[4] P. Clavin, Proc. Combust. Inst. 28, 569 (2000).

[5] P. Clavin and G. Joulin, J. Phys. Letters 44, L-1 (1983).

[6] S. G. Davis, J. Quinard and G. Searby, Combust. Flame 130, 112 (2002); ibid. 123 (2002).

[7] L. K. Tseng, M. A. Ismail and G. M. Faeth, Combust. Flame 95, 410 (1993).

[8] B. Deshaies and P. Cambray, Combust. Flame 82, 261 (1990).

[9] B. Lewis and G. von Elbe, J. Chem. Phys. 11, 75 (1943).

[10] M. S. Uberoi, J. Chem. Phys. 22, 1784 (1954).

[11] R. M. Fristrom, J. Chem. Phys. 24, 888 (1956).

[12] M. S. Uberoi, A. M. Kuethe and H. R. Menkes, Phys. Fluids 1, 150 (1958).

[13] M. S. Uberoi, Phys. Fluids 2, 72 (1959).

[14] M. S. Uberoi, Phys. Fluids 6, 1104 (1963).

[15] M. S. Uberoi and A. Zimmerman, Phys. Fluids 8, 1628 (1965).

[16] J. Menkes, Combust. Flame 4, 1 (1960).

[17] S. B. Berndt, J. Fluid Mech. 26, 433 (1966).

[18] G. E. Andrews and D. Bradley, Combust. Flame 18, 133 (1972).

[19] S. Noda, T. Nakajima, S. Maeda, K. Kimoto and R. Matsumoto, Bull JSME 27, 749 (1984).

[20] J. Buckmaster, Physica D 20, 91 (1986).

[21] B. Lewis and G. von Elbe, *Combustion, Flames and Explosions of Gases,* Academic Press, Orlando, 1987, chapter 5.

[22] M. Z. Pindera and L. Talbot, Combust. Flame 73, 111 (1988).

[23] A. Fines, T. Tsuruda and T. Hirano, Combust. Flame 95, 76 (1993).

[24] N. Z. Squires and P. A. Libby, Combust. Sci. Technol. 103, 21 (1994).

[25] M. Matalon, C. Cui and J. K. Bechtold, J. Fluid Mech. 487, 179 (2003).

[26] M. J. Remie, M. F. G. Cremers, K. R. A. M. Schreel and L. P. H. Goey, Combust. Flame 147, 163 (2006).

[27] M. Matalon, Ann. Rev. Fluid Mech. 39, 163 (2007).

[28] F. J. Higuera, Combust. Flame 156, 1063 (2009).

[29] K. C. Kim, S. Y. Yoon, S. M. Kim, H. H. Chun and I. Lee, Experiments in Fluids 40, 876 (2006).

[30] Y.-C. Chen, M. Kim, J. Han, S. Yun and Y. Yoon, Proc. Combust. Inst. 31, 1327 (2007).